Large-Grain Formamidinium $PbI_{3-x}Br_x$ for High-Performance Perovskite Solar Cells via Intermediate Halide Exchange

Mingzhu Long, Tiankai Zhang, Wangying Xu, Xiaoliang Zeng, Fangyan Xie, Qiang Li, Zefeng Chen, Fengrui Zhou, Kam Sing Wong, Keyou Yan, and Jianbin Xu**

Formamidinium lead iodide $FAPbI_3$ or itsmixed perovskite solar cells (PSCs) have received considerable interest recently because of their high efficiency, low hysteresis, and notable photoaging stability.[1] Large-area perovskite devices with high efficiency, prepared using the solution process, were demonstrated to potentially outperform traditional thin-film photovoltaic technology, displaying promising industrial viability.[2] $FAPbI_3$ displays a low open-circuit voltage (V_{oc}) due to a narrow band gap and suffers from a transition to a yellow non-perovskite phase (δ-$FAPbI_3$) at room temperature (RT). As an important milestone, Seok and co-workers incorporated $MAPbBr_3$ into $FAPbI_3$ to forming a mixed perovskite with a stable black α-phase at RT.[2b] Afterwards, Zhao and co-workers reported the deposition of high-quality $FAPbI_3$ thin films by using FAI and the intermediate HI-adduct $HPbI_3$.[3] This conversion process probably involves the decomposition of FAI, followed by reaction of FA with $HPbI_3$, which necessitates a long sintering time of 90 min to release the excess iodide. In addition, an intramolecular exchange of dimethyl sulfoxide (DMSO) of the intermediate PbI_2-DMSO solvate with FAI was developed for high-quality $FAPbI_3$, which improved the morphology and delivered a high efficiency, above 20%.[1a] These final products still have a phase instability problem under humidity.[4]

In these solution routes, a crucial step is the dripping of a large amount of antisolvent/nonsolvent to prevent the formation of intermediate anisotropic fibers of "FAI-PbI_2-DMSO/DMF" solvate adduct, so that highly compact and homogeneous thin films can be produced.[1a] This dripping process should be performed within 1–2 s of the nucleation stage during spin-coating, which requires skilled operation. Otherwise, a radial gradient of non-uniformity on the film surface results, with a wide distribution of device performance in different batches. Recently, Li et al. reported a vacuum-flash-assisted solution process to overcome this shortcoming.[5] However, the immediate post-treatment using vacuum-flash increases the operation complexity and variability. Thus, alternative procedures for the solution methods need to be developed to prepare uniform perovskite thin films without requiring the "dripping" and/or post-treatment. Such a development will provide an advantage over the competing vacuum deposition technology in inorganic thin-film photovoltaics.[6]

In this work, we develop a halide-exchange process (HEP) reaction that uses nonstoichiometric 1.3:1 FAI: $HPbI_2Br$, which enables the deposition of large-grained and compact $FAPbI_{3-x}Br_x$ thin films without using antisolvent dripping during spin coating. We reveal the crystallographic conversion process in association with this intermediate and demonstrate the reliability of the HEP reaction through simple nonstoichiometric co-ordination control. The structure of the intermediate $HPbI_2Br$ features a hexagonal array of $[PbI_2Br]^-$ anionic columns similar to those found in $[PbI_3]^-$ in δ-$FAPbI_3$, with Br partially replacing the iodine in the stacked tripods. Br substitution makes the anionic column/chain unstable, which facilitates its exchange by iodine and release of the residue in the HEP reaction. We find that the reduced bromide also promotes the intermediate conversion into stable and high-quality $FAPbI_{3-x}Br_x$. In addition, excess halide prevents the formation of an anisotropic morphology during the spin-coating process and heals the grain boundary afterwards, which delivers large and compact grains up to 2–3 μm. Perovskite devices produced by the HEP exhibit a stable efficiency as high as 19.0% for the reverse scan and demonstrate high reproducibility. Therefore, this HEP provides a lower entry level from which to achieve high efficiency without the antisolvent dripping process, which brings about industry viability and reliability after further optimization.

The HEP is schematically illustrated in **Figure 1**A, which involves the use of the intermediate compound $HPbI_2Br$ and the non-stoichiometric 1.3:1 FAI: $HPbI_2Br$ precursor to produce the mixed perovskite. The intermediate $HPbI_2Br$ was fabricated by mixing PbI_2/HBr in dimethyl formamide (DMF), stirring at 40 °C overnight to eliminate the undesirable remnant PbI_2. Pale yellow powder is obtained (Figure S1A, see Supporting Information, left inset) by precipitation with excess diethyl ether. Figure 1B and S1A display scanning electron microscope (SEM) images of the $HPbI_2Br$, with a crystal morphology similar to hexagonal prisms attached to each other. The intermediate

M. Z. Long, T. K. Zhang, Z. F. Chen, Prof. K. Y. Yan, Prof. J. B. Xu
Department of Electronic Engineering
Chinese University of Hong Kong
Shatin, New Territories, Hong Kong
E-mail: kyyan@ee.cuhk.edu.hk; jbxu@ee.cuhk.edu.hk
Prof. W. Y. Xu
College of Materials Science and Engineering
Shenzhen University
Shenzhen 518060, P. R. China
X. L. Zeng, F. R. Zhou
Shenzhen Institute of Advanced Technology
Chinese Academy of Science
Shenzhen 518055, P. R. China
Prof. F. Y. Xie
Instrumental Analysis and Research Center
Sun Yat-sen University
Guangzhou 510275, P. R. China
Dr. Q. Li, Prof. K. S. Wong
Department of Physics
Hong Kong University of Science & Technology
Clear Water Bay, Kowloon, Hong Kong

DOI: 10.1002/aenm.201601882

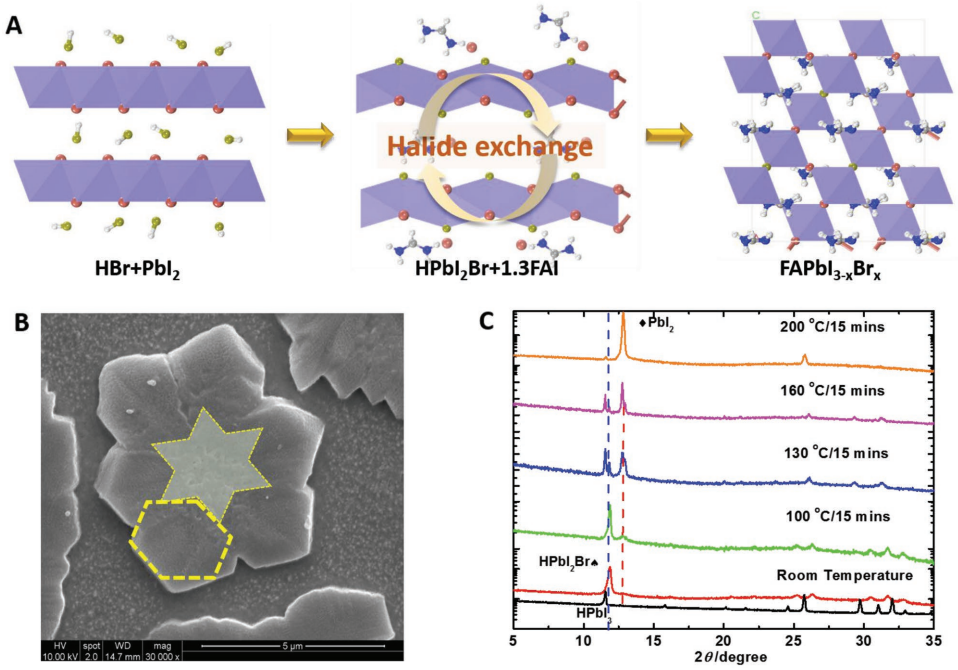

Figure 1. Halide exchange scheme and the characterization of intermediate $HPbI_2Br$. A) Schematic illustration of intermediate synthesis and its halide exchange for $FAPbI_{3-x}Br_x$ perovskite. B) SEM image of $HPbI_2Br$. C) XRD pattern for $HPbI_2Br$ thin film and its instability evolution under heating.

$HPbI_2Br$ has similar $[PbX_3]^-$ framework arrays as well-known δ-$FAPbI_3$ and our $HPbI_3$ ($P6_3mc$ space group, No: 186, Figure S2) reported in previous work.[7] The peak at $2\theta = 11.9°$ in the X-ray diffraction (XRD) pattern corresponds to the (100) facet of the as-prepared $HPbI_2Br$ thin film (Figure 1C). We checked the structural stability of the $HPbI_2Br$ by monitoring the XRD patterns of the thin films after sintering at different temperatures (Figure 1C) and found the appearance of a peak at $2\theta = 12.6°$, which indicates conversion into hexagonal PbI_2, even after sintering at 100 °C. Based on the structure of $[PbX_3]^-$ (Figure S2) after partial Br replacement in the $[PbI_3]^-$ columns, the as-formed $HPbI_2Br$ is not thermally stable due to the lower asymmetry of the Pb–X framework than of $HPbI_3$; this disparity has the potential to facilitate the reaction between the intermediate and FAI through I/Br exchange for conversion into the optimally mixed halide perovskite (reaction 1). In addition, the feasibility of bromide release should guarantee that the $HPbI_2Br$ can be used as an effective mediator reactant to replace PbI_2 and retard the reaction. The excess halide prevents the fast self-assembly crystallization process from forming FAI–PbI_2–DMF ($FAPbI_3$ DMF) and then the perovskite by direct mixing of PbI_2 and FAI (reaction 2). Moreover, the slight Br-doping inhibits the back conversion into the non-perovskite yellow phase and stabilizes the final perovskite phase.[1a] From the analysis above, the HEP reaction through the intermediate $HPbI_2Br$ and the conventional fabrication of $FAPbI_3$ can be described as:

$$1.3FAI + HPbI_2Br + DMF \xrightarrow{HEP} FAPbI_{3-x}Br_x \cdot DMF \xrightarrow{heating} FAPbI_{3-x}Br_x \quad (1)$$

$$FAI + PbI_2 \xrightarrow{DMF} PbI_2 \cdot FAI \cdot DMF \xrightarrow{-DMF} \delta FAPbI_3 \xrightarrow{heating} \alpha FAPbI_3 \quad (2)$$

The UV-vis absorption spectra for the $HPbI_2Br$ and the other mixed precursors are shown in Figure S1B. $HPbI_2Br$ displays an approximately 25 nm red shift of the absorption plateau edge (490 nm) with respect to that of the pure PbI_2 precursor, which suggests that it is a new co-ordination lead complex.[8] After adding FAI into the precursor $HPbI_2Br$, the absorption edge has an only 5-nm red-shift relative to that of pure $FAPbI_3$ precursor, which confirms the further co-ordination by FAI with the intermediate $HPbI_2Br$.

To check the evolution of the halide exchange and conversion of the intermediate product to perovskite in the HEP reaction, we first monitored the color of the thin films and changes in the UV-vis absorption as a function of sintering time at 160 °C, as shown in **Figure 2**A,B. The full conversion takes approximately 60 min to yield a mirrorlike perovskite thin film (Figure S3), based on color and absorption monitoring. The detailed conversion process can be divided into two main transformative stages. For samples of RT and 1 min, the transparent yellow thin films display a very low absorbance in the UV-vis spectra due to the DMF solvate complex, which corresponds to $FAPbI_{3-x}Br_x$ DMF. For the sample sintered for 5 min, the absorbance below 500 nm increases quickly and a new peak appears at 470 nm in the UV-vis spectrum, which may be attributed to an unsolvated intermediate complex formed after DMF removal. After a sintering time of 20 min, the absorption onset approaches 1.51 eV (810 nm), which indicates the start of the conversion from the unsolvated intermediate complex into the $FAPbI_{3-x}Br_x$ perovskite. With a sintering time of 40–60 min, the disappearance of the absorption at 470 nm may indicate the gradual completion of the perovskite reaction. The slightly larger band-gap than is the case for $FAPbI_3$ (1.47 eV) obtained from the UV-vis spectrum is ascribed to incorporation

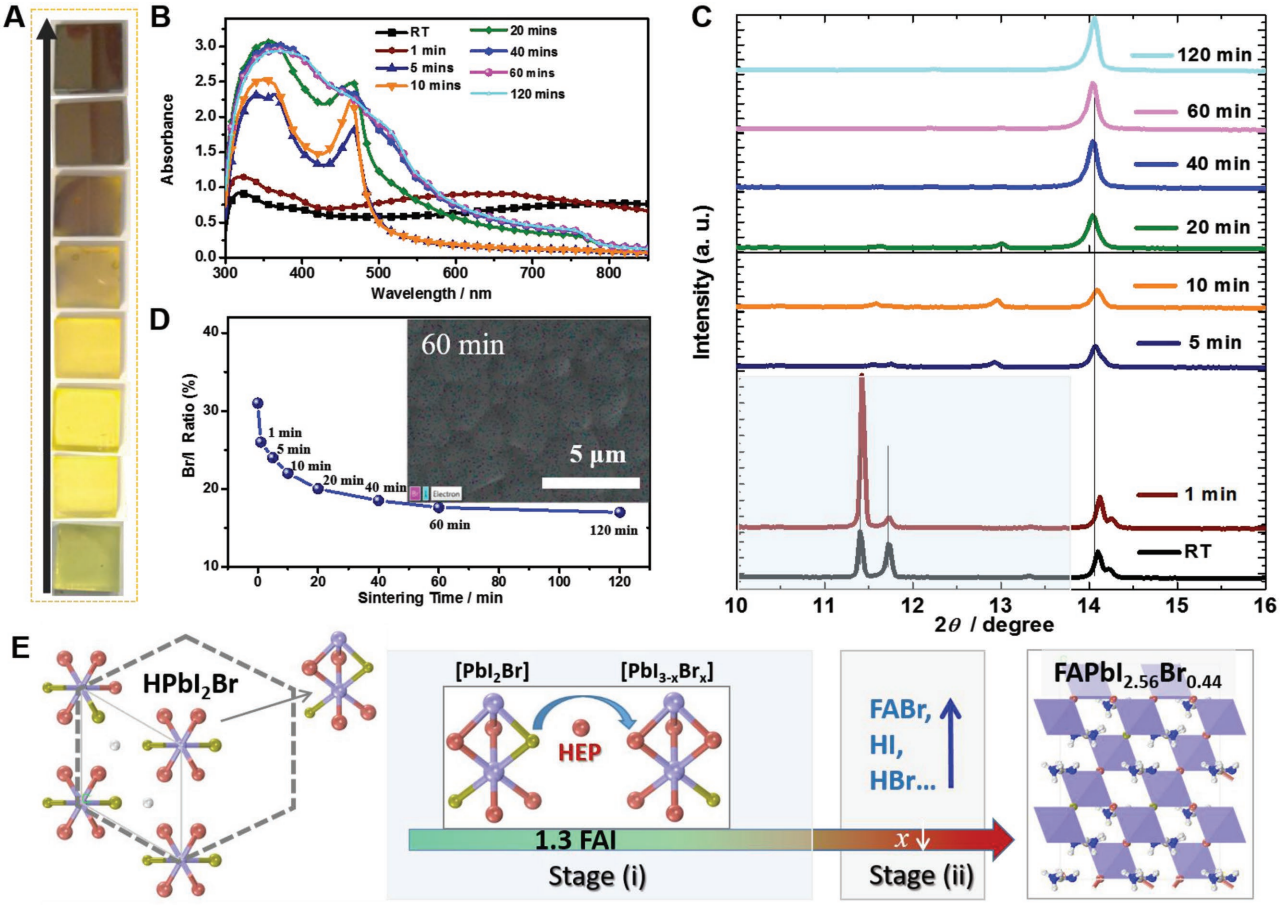

Figure 2. HEP evolution and crystallographic conversion. A) Thin-film color change, B) UV-vis absorption, C) XRD patterns, and D) Br/I atomic ratio from XPS, for evolution investigation of the films under heating (inset: EDX mapping of the sample after 60 min annealing). E) Crystallographic conversion illustration: i) $[PbI_2Br]$ converts into $[PbI_{3-x}Br_x]$ inorganic framework in the presence of FAI through HEP reaction; ii) impurity removal including phase conversion and impurity volatilization.

of Br.[1a] Further increasing the sintering time to 120 min did not change the absorption onset wavelength and demonstrated robust thermal stability as well.

To identify the exact phase transformation process in the different stages, we used XRD in combination with X-ray photoelectron spectroscopy (XPS; Figure 2C and 2D). We found an XRD peak at $2\theta = 11.9°$ that is indicative of $HPbI_2Br$ shifts to lower angle for the freshly spin-cast sample in Figure 2C, which suggests the intercalation of FAI and DMF into $HPbI_2Br$ and a transformation to $FAPbI_{3-x}Br_x$ DMF ($x < 1$) solvates similar to the reported $MAPbI_3$ DMF or $FAPbI_3$ DMF.[9] The solvates formed from the HEP reaction have two peaks at $2\theta = 11.7°$ and 11.4°. After annealing for 1 min, we observed a large increase of the intensity of the peak at $2\theta = 11.4°$ accompanied by the substantial attenuation of the peak at $2\theta = 11.7°$, due to the further substitution of bromine by the larger iodine by means of halide exchange. After 5 min annealing, this $FAPbI_{3-x}Br_x$ DMF solvate quickly converts into $FAPbI_{3-x}Br_x$ perovskite, based on the increasing perovskite ($\bar{1}11$) peak and the disappearance of the peaks at $2\theta = 11.4°$ and 11.7° due to DMF removal. The detailed XPS spectra for Br-evolution are shown in Figure 2D and Figure S5. The peaks at binding energies (BE) of 67.8 and 68.9 eV are assigned to Br $3d_{5/2}$ and $3d_{3/2}$, with the Br/I molar ratios shown in Figure 2D. In combination with the large Br loss, as judged from XPS monitoring of the fresh and 1 min samples, this provides further evidence for the substitution of bromine with iodide through the HEP reaction. The nonstoichiometric FAI/$HPbI_2Br$ precursor converts into $FAPbI_{3-x}Br_x$ DMF solvates through the HEP reaction, as illustrated in Figure 2E, partially losing excess Br in the transient state to form a more stable structure. The release of DMF from the solvate can be also ascertained from the disappearance of the oxygen peak of the XPS spectra in Figure S5A. After further calcination, the excess Br is removed, as can be verified by the decreased Br concentration in the perovskite crystallization state in Figure 2D.

The sample annealed for 10–20 min at 160 °C has an XRD peak at 14.10°, which is indicative of the perovskite phase but the corresponding photographs of the thin film in Figure 2A show that it is still yellowish. The similar yellowish intermediate has also been reported in the 3:1 MAI: $PbCl_2$ recipe for $MAPbI_{3-x}Cl_x$ during the perovskite transition; this coloration is attributed to the halide-rich species.[10] The gradual removal of Br can also be confirmed by the slight shift of the ($\bar{1}11$)

diffraction peak from 14.10° to 14.02° during the transitional stage after annealing for 5–20 min. After annealing for more than 60 min, all the excess halide is removed, which leads to full conversion of the starting compound into a well-crystallized $FAPbI_{3-x}Br_x$ perovskite. Therefore, due to the facile removal of FABr compared to that of FAI, as seen in the thermogravimetric analysis (TGA curves in Figure S4), the bromide in the HEP reaction can be removed easily and selectively in the transitional stages, which leads to stable $FAPbI_{3-x}Br_x$ perovskite. After 60 min of sintering, the Br/I ratio in the final film is constant at 17.2%. This ratio indicates that x is 0.44, which corresponds to the molecular formula of $FAPbI_{2.56}Br_{0.44}$. The energy-dispersive X-ray (EDX) element mapping confirms the uniform distribution of bromine and iodine in the film, as shown in Figure 2D inset. The final atomic ratio Br/I measured from the EDX analysis (EDX mapping and spectrum in Figure S6) is 17.9%, which is consistent with the ratio from the XPS results.

HEP delivers a compact surface morphology and a large crystal size up to 2–3 µm for $FAPbI_{3-x}Br_x$, as seen from the SEM image in **Figure 3**A; the crystal size is substantially larger than that prepared from other solution processes. In conventional $FAPbI_3$, with the assistance of the antisolvent, a compact surface is seen but with a much smaller crystal domain due to the quick nucleation, as seen in Figure 3B. Without the antisolvent, the film coverage is quite poor, with a hexagonal column crystal morphology induced by the parent solvate adducts (Figure 3B inset). Therefore, in the HEP method, the geometric instability of the $HPbI_2Br$ complex and excess FAI facilitate the full coverage and phase conversion to $FAPbI_{3-x}Br_x$ perovskite, excluding the formation of anisotropic structures in the excess-halide environment. The pinhole-free microstructure and large domain of the grains are further supported by the atomic force morphology (AFM) images in Figure 3C1 and Figure S8, which show the grain boundary and the interior more clearly, with the largest crystal size being around 3 µm. The corresponding Kelvin probe force microscopy (KPFM) analysis of the HEP film shows that the boundary and interior potential difference is negligible in Figure 3C2, which means that the grain boundary does not act as a defect site for detrimental trap-mediated recombination. We speculate that charge recombination can be minimized at the grain boundaries formed by the HEP reaction, where the nonradiative recombination losses are most likely to occur. The large grains favor long-range charge transport,[11] which can lead to high-efficiency PSCs. There are numerous studies about the significant role of chloride or bromide in $MAPbI_{3-x}Cl_x$/$MAPbI_{3-x}Br_x$ in improving the perovskite crystallization and optoelectronic properties.[12] However, for the FA-cation-based perovskite, we did not choose chloride because of both the thermal and the humidity instability problems of $FAPbI_{3-x}Cl_x$.[13] Therefore, we stress the importance of the effect of excess bromide on the crystallization and the improved electronic properties of the mixed-halide $FAPbI_{3-x}Br_x$.

The HEP method produces high film crystallinity compared with conventional direct mixing (Figure 3D). The intermediate complex is fully converted into a more textured film than is the case for the control film, with a higher preferred orientation of the perovskite and a main peak of $(\bar{1}11)$ facet at 14.02°. Compared to the $(\bar{1}11)$ peak of $FAPbI_3$ at 13.90°, the main XRD peak of $FAPbI_{3-x}Br_x$ is shifted towards a higher value of 2θ.[1a] The

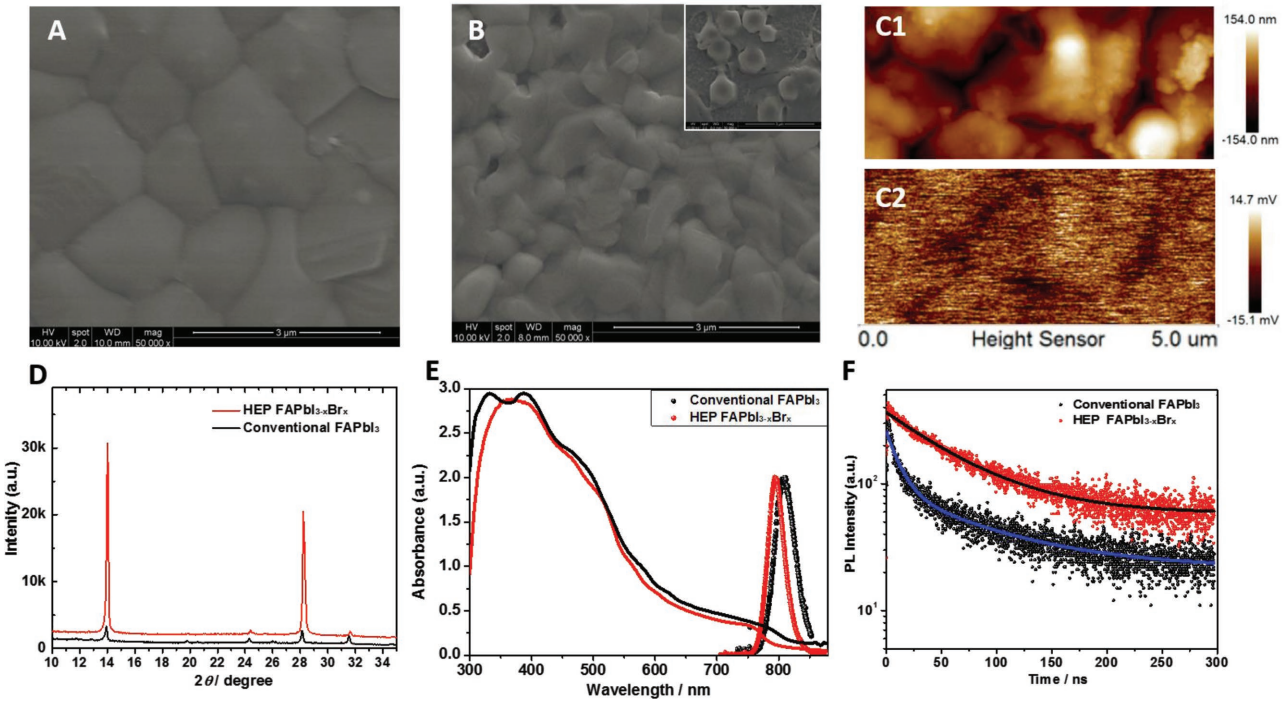

Figure 3. Film quality characterizations. A) SEM image of $FAPbI_{3-x}Br_x$ perovskite by HEP reaction, B) SEM image of $FAPbI_3$ perovskite with and without dripping (inset), C) AFM and KPFM profiles of $FAPbI_{3-x}Br_x$ perovskite, D) XRD patterns comparison, E) UV-vis absorption, steady-state PL, and F) TRPL spectra for $FAPbI_{3-x}Br_x$ and conventional $FAPbI_3$ perovskite thin films.

shift of the main peak to higher values of 2θ demonstrates the effect of doping of the smaller Br atoms and the decreased lattice spacing in the final $FAPbI_{3-x}Br_x$ perovskite. In addition, the intensity of the main peak of $FAPbI_{3-x}Br_x$ is also enhanced by several orders of magnitude compared to that of $FAPbI_3$. This result is attributed to excess halide in the precursor; the gradual release of excess bromide ameliorates the crystallization, leading to a preferential orientation during crystallization in the HEP reaction. We also did the control experiment through the addition of HBr aqueous solution into $FAPbI_3$ to monitor the effect of excess Br with a molar ratio of $FAPbI_3$:HBr = 1:0.55. From the XRD patterns in Figure S7, we can see that intensity of the main peak is decreased compared to that of pure $FAPbI_3$. This decrease could be attributed to the existence of substantial H_2O in the aqueous HBr acid, which leads to low crystallinity.

To gain further insight into the effect of the HEP reaction on the perovskite film quality, we characterized the optoelectronic behaviors of the perovskite thin film by steady-state photoluminescence (PL) spectrometry and nanosecond time-resolved PL (TRPL) decay, as shown in Figure 3E and 3F. The steady-state PL spectral peak is at 795 nm for $FAPbI_{3-x}Br_x$ and shows a much smaller Stokes shift compared to that of conventional $FAPbI_3$, with an emission at 807 nm. The absorption band edges are 810 and 840 nm for $FAPbI_{3-x}Br_x$ and $FAPbI_3$ separately. This result illustrates the milder vibronic relaxation and reduced crystallization defects of the HEP perovskite film.[14] The full width at half maximum (FWHM) from the PL spectra are 37 and 53 meV for the HEP $FAPbI_{3-x}Br_x$ and conventional $FAPbI_3$ thin film, respectively. The TRPL characterization of the perovskite films is shown in Figure 3F. The carrier lifetimes are τ_1 = 67.5 ns and τ_2 = 11.20 ns for the HEP $FAPbI_{3-x}Br_x$ and the conventional $FAPbI_3$, respectively. The combination of decreased blue-shift of the band-edge PL, smaller FWHM, and longer lifetime of the HEP $FAPbI_{3-x}Br_x$ demonstrate that there is much less nonradiative recombination than for the control sample, owing to the larger crystal domains via deliberate HEP. Therefore, we can conclude that HEP delivers much higher quality perovskite than the conventional route, with a larger grain size, higher crystallinity, and better optoelectronic properties.

We then fabricated devices consisting of fluorine-doped tin oxide (FTO)–glass/blocking layer(bl)–TiO_2/perovskite/Spiro-OMeTAD/Au (n–i–p architecture). **Figure 4**A shows the photocurrent–voltage (J–V) curves of PSCs fabricated with $FAPbI_{3-x}Br_x$ made with the HEP reaction and PSCs fabricated with conventional $FAPbI_3$ made by dripping, measured under a simulated air mass of 1.5 (AM 1.5; one sun light, 100 mW cm^{-2}) with reverse and forward scanning directions. The detailed performance parameters, including short-circuit current (J_{sc}), V_{oc}, fill factor (FF), and PCE, are listed in Table S1. The J–V curve of HEP gives V_{oc} = 1.09 V, J_{sc} = 22.99 mA cm^{-2}, and FF = 0.758 in the reverse scan, and V_{oc} = 1.06 V, J_{sc} = 22.91 mA cm^{-2}, and FF = 0.719 in the forward scan, which correspond to PCE values of 19.0% and 17.5%, respectively, with negligible hysteresis. Conventional $FAPbI_3$ perovskite has a much lower PV performance and a larger hysteresis, with V_{oc} = 0.99 V, J_{sc} = 21.04 mA cm^{-2}, and FF = 0.646 in the reverse scan, which amounts to a PCE of 13.5%. The PSC fabricated with $FAPbI_{3-x}Br_x$ produced from the HEP reaction has much higher FF and V_{oc} values than those of $FAPbI_3$. The Br doping can enlarge the V_{oc} value to some extent, and the J_{sc} value is increased despite the absorption edge of the $FAPbI_{3-x}Br_x$ shift to 810 nm compared to the 840-nm value of $FAPbI_3$. This increased current could be accounted for by the ameliorative carrier transport in the well-crystallized $FAPbI_{3-x}Br_x$ perovskite thin film. 80 cells were fabricated to study the reproducibility of this HEP reaction and conventional $FAPbI_3$, as seen in Figure 4B. The efficiencies of the cells with the HEP perovskite exhibit a smaller relative standard derivation than the control method (1.79 vs. 4.83). The average efficiency of the group with the HEP perovskite (17.42%) is much higher than that of the group with conventional $FAPbI_3$ (9.78%), which reveals that the HEP method for perovskite devices is much more reliable and reproducible, even without the assistance of antisolvent.

The J–V performance of the champion cell is shown in Figure 4C, with device parameters in Table S1. In reverse scan the cell has values of V_{oc} = 1.10 V, J_{sc} = 23.0 mA cm^{-2}, and FF = 0.760, which correspond to a PCE of 19.20%. In Figure 4D we show the maximum output of the champion $FAPbI_{3-x}Br_x$ device under constant illumination with bias voltage (0.88 V). The stabilized output from this tracking curve is 18.35%, which is consistent with the value from the J–V curve. To demonstrate the film quality in the integrated device, we show the cross-sectional SEM image for the fabricated devices in Figure 4E. The device with the $FAPbI_{3-x}Br_x$ film derived from the HEP reaction exhibits a compact and well-developed grain structure with a crystal domain size as large as 2–3 μm and a film thickness of approximately 390 nm. Such a large single-crystal grain in the HEP perovskite device can directly contact with the carrier selective layers, as seen from the cross-sectional image. It can be inferred that most of the photogenerated carriers can effectively reach the electrodes without encountering grain boundaries, which should significantly enhance charge collection in the operating device. Such a large crystal size and compact microstructure were not reported for FA-based perovskite thin films, which suggests a large step towards a high-quality PSC.

Beyond the improved film quality and device efficiency, the HEP method also endows the perovskite films with promising moisture and thermal stability. XRD patterns and color evolution of thin films were monitored to observe the degradation process for the perovskite produced from the HEP reaction. The HEP thin film can maintain the mirrorlike black surface after storing for up to six weeks in a cabinet with 60 ± 5% humidity, and no impurity phases are observed in the XRD patterns, as shown in Figure 4F. Due to the polymorph of the stable non-perovskite phase of $FAPbI_3$ at RT, it becomes yellow in less than two days under similar conditions. In the HEP reaction, the intermediate $HPbI_2Br$ has a higher co-ordination number than that of PbI_2. Therefore, it reduces the co-ordination of DMF to Pb(II) and retards the perovskite crystal growth, which results in large crystal domains with fewer defects in the $FAPbI_{3-x}Br_x$ lattice.[15a] This result can decrease the probability of H_2O penetration through the vacant sites and grain boundaries, and account for the enhanced humidity stability.[15] The thermal stability of the FA-only based perovskite is very high, as seen in Figure 4G. The main peak of $FAPb_{3-x}Br_x$ becomes even stronger for the thin film stored at 85 °C for 240 h, without any

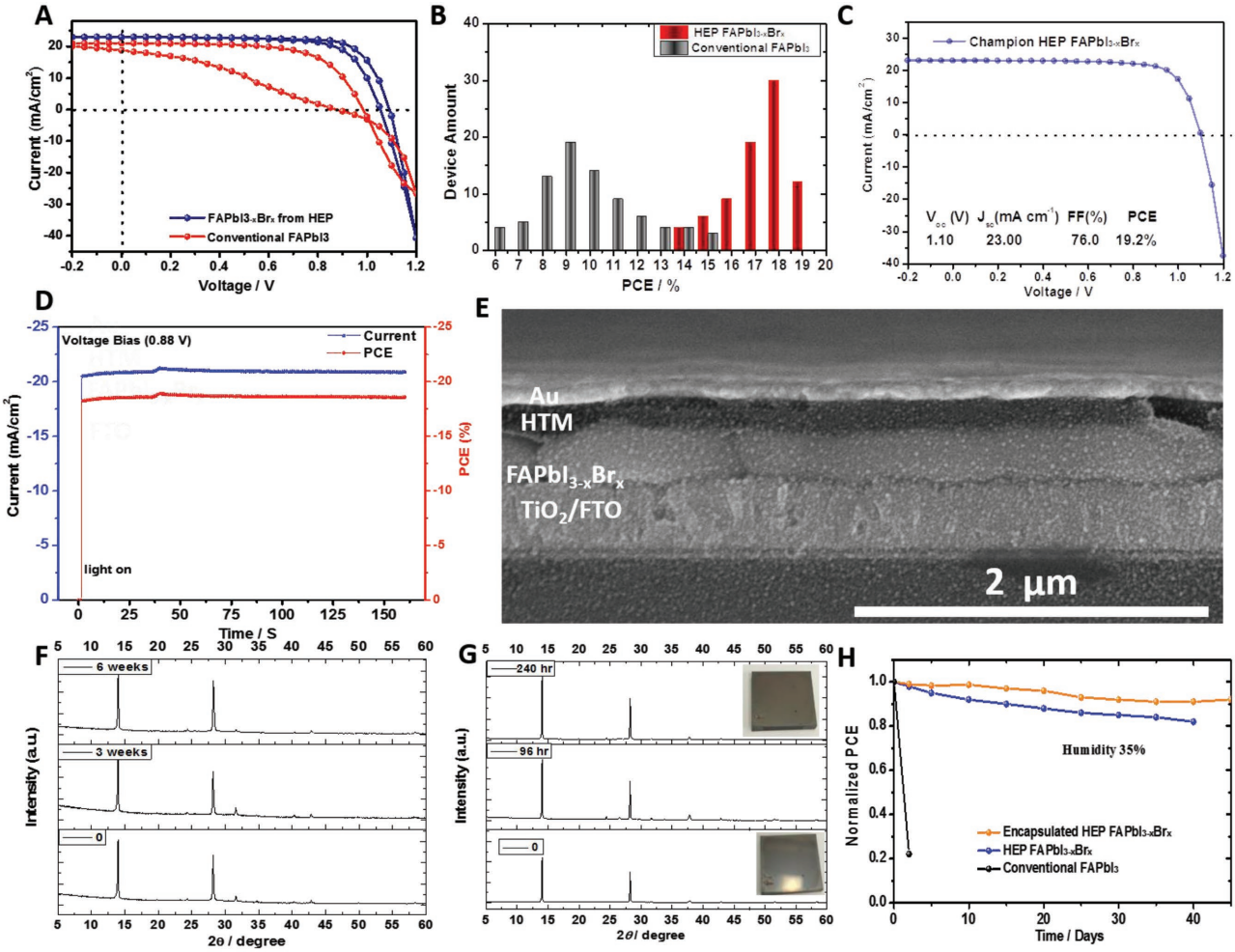

Figure 4. Performance metrics. A) *J–V* performance with a cell area of 0.15 cm^2 and B) PCE distribution for HEP $FAPbI_{3-x}Br_x$ and $FAPbI_3$, C) champion cell performance, D) steady state output at a maximum power point (0.88 V) for the champion device, E) SEM image of the device cross-section, F) humidity-stability characterization for the bare thin film at 60 ± 5% RH, G) thermal stability characterization for the bare thin film at 85 °C, H) device-stability comparison between HEP, encapsulated, and control $FAPbI_3$ devices in 35 ± 2% RH.

notable impurity peaks. In contrast, the mixed $FA_{0.85}MA_{0.15}Pb(I_{0.85}Br_{0.15})_3$ perovskite (Figure S9) gradually turns yellow after storage in the same conditions for 192 h. Therefore, although there are many reports about the performance improvement for the perovskite by mixing FA with the MA cation, FA only or FA-Cs mixed perovskites still have an advantage over their MA mixed counterpart in terms of thermal stability.[16] As shown in Figure 4H, we also investigated device stability under long-term humidity in a cabinet with the humidity controlled at 35 ± 2% at RT under room-light illumination. The $FAPbI_{3-x}Br_x$ device from the HEP reaction maintained an efficiency of 80% after 40 days of storage without encapsulation. After encapsulation, the efficiency was maintained at 92% of the initial performance after 50 days.

We demonstrate that the HEP reaction between the intermediate $HPbI_2Br$ and nonstoichiometric FAI is a reliable method to prepare $FAPbI_{3-x}Br_x$ perovskite, and eliminates the need for antisolvent dripping. The unstable intermediate can facilitate the HEP reaction and enlarge the crystal domain in the perovskite by gradually releasing excess bromide. The HEP reaction influences the crystallization kinetics, favoring a higher quality organic–inorganic compound. As a result, a highly orientated and compact thin film with large crystalline grains is achieved. This high-quality film leads to a PSC device with an efficiency of up to 19.0% without appreciable hysteresis, with improved humidity and thermal stability properties, and this HEP method also increases the reproducibility. This successful HEP reaction opens an alternative method to improve the thin film quality, instead of the rapid crystallization kinetics by the direct-mixing method, and it also demonstrates a reliable way of doping with Br to stabilize the perovskite phase for high-efficiency PSCs.

Experimental Section

Materials: Formamidinium iodide (FAI, Dyesol), PbI_2 (Sigma-Aldrich, 99%), *N*,*N*-dimethylformamide (Sigma-Aldrich, anhydrous, 99.8%),

Spiro-OMeTAD (Merck), 4-tert-butylpyridine (4-TBP, Sigma-Aldrich, 96%), titanium(IV) isopropoxide (Sigma-Aldrich, 99.999%), niobium ethoxide (Sigma-Aldrich, 99.95 wt%), hydrobromic acid (HBr, 48 wt%), lithium bistrifluoromethane-sulfonimidate (LiTFSI, Sigma-Aldrich, 99.95%), chlorobenzene (Sigma–Aldrich, anhydrous, 99.8%), and all other chemicals were used as received without further purification.

$HPbI_2Br$ Preparation: HPb_2Br powder was prepared by mixing PbI_2 (4.62 g) and 48 wt% HBr (1.6 mL) in DMF (10 mL) to ensure complete conversion, and stirring at 40 °C overnight. The light-yellow precipitate was obtained by washing the precursor in abundant diethyl either to remove excess HBr, until the supernatant turned clear. The obtained powder was dried and stored in an oven at 60 °C.

Device Preparation: F-doped SnO_2 (FTO) (Tec8) substrates were cleaned in an ultrasonic bath sequentially with acetone, 2-propanol, and ethanol for 15 min, respectively. The TiO_2 precursor was prepared by mixing titanium isopropoxide (0.6 mL) and of 37 wt% HCl (0.15 mL) solution dissolved in ethanol (15 mL), with 5 mol% Nb doping with niobium ethoxide. The dense TiO_2 blocking layer was coated onto the FTO substrate by spin-coating the titanium precursor at 6500 rpm for 30 s, followed by annealing in air at 500 °C for 30 min. FAI and $HPbI_2Br$ were dissolved in DMF with a molar ratio of 1.3:1 and then the precursor was spin-coated on the TiO_2 substrates for solar cell fabrication. The fresh thin film is brilliant yellow, and gradually turns dark brown and with a mirrorlike surface after baking at 160 °C for around 60 min.

The spiro-OMeTAD was prepared by dissolving spiro-OMeTAD (56 mg) with LiTFSI solution (520 mg in 1 mL acetonitrile, 25 µL), and TBP (35 µL) in chlorobenzene (1 mL) and stirred at 40 °C overnight. The hole transport layer was deposited on the annealed perovskite film by spin-coating at 6500 rpm for 40 s to obtain the optimized efficiency. The devices were placed in a moisture-controlled cabinet overnight for oxidization of spiro-OMeTAD. Finally, an 80 nm-thick Au electrode was deposited by thermal evaporation with a shadow mask area of 0.15 cm^2.

Stability Experiments: For all of the humidity stability studies, the perovskite films were stored at RT (measured as 25 ± 1 °C) in controlled-humidity cabinets with a transparent glass door, with a normal fluorescent light in the room. The relative humidity in the chambers were controlled to the desired humidity of 60 ± 5% or 35 ± 2% for the thin film and device stability test, respectively. The relative humidity in the cabinet was precisely measured periodically throughout the stability experiments by using a calibrated hygrometer.

Characterization: The extinction and UV-vis absorption spectra of solution samples were measured on a Hitachi U-3501 UV/visible/NIR spectrophotometer. The micrographs of the film morphology were obtained using an FEI Quanta 400 field-emission scanning electron microscope (FESEM, FEI, Quanta 400 FEG) operated at 10 keV. X-ray diffraction (XRD) measurements were conducted with a Bruker D8 Advance Davinci powder X-ray diffractometer using a Cu Kα source. The current density–voltage curves of solar cells were measured (Keithley Instruments, 2612 Series Source Meter) under the simulated AM 1.5 sunlight generated by a 94011A-ES Sol Series Solar Simulator. A calibrated silicon diode with a known spectral response was used as the reference. Thermal analyses were carried out with a thermogravimetric analyzer (PerkinElmer, TGA 6) with ramp rate of 5 °C min^{-1}. The elemental composition of the perovskite was measured by using X-ray photoelectron spectroscopy (XPS) (Thermo Fisher Scientific, ESCALAB 250). Time-resolved photoluminescence (TRPL) spectra of the perovskite samples were measured by using a Hamamatsu Steak Scope C4334 apparatus. Femtosecond pump pulses were provided by the Coherent Model Mira 900 titanium: sapphire laser. The average pump intensity at the sample was approximately 28 µW with 150 fs pulse. The PL lifetimes of the perovskite thin films deposited on glass were calculated by fitting the transient data to the single-exponential decay. The time-resolved PL signal was collected by a TCPSC system. The steady state PL was also characterized with an excitation wavelength of 710 nm and a average excitation intensity of 103 µW $pulse^{-1}$. CCDC 1479488 contains the supplementary crystallographic data for this paper. These data can be obtained free of charge from The Cambridge Crystallographic Data Centre via www.ccdc.cam.ac.uk/data_request/cif.

Supporting Information

Supporting Information is available from the Wiley Online Library or from the author.

Acknowledgements

M.Z.L. and T.K.Z. contributed equally to this work. The work is supported in part by the Research Grants Council and the Innovation and Technology Fund of Hong Kong, particularly via Grant Nos. AoE/P03-08, 14204616, T23-407/13-N, ITS/004/14, HKUST 606511, 605710, AoE/P-02/12 and CUHK Group Research Scheme.

Received: August 25, 2016
Revised: November 16, 2016
Published online:

[1] a) W. S. Yang, J. H. Noh, N. J. Jeon, Y. C. Kim, S. Ryu, J. Seo, S. I. Seok, *Science* **2015**, *348*, 1234; b) N. Pellet, P. Gao, G. Gregori, T. Y. Yang, M. K. Nazeeruddin, J. Maier, M. Grätzel, *Angew. Chem. Int. Ed.* **2014**, *53*, 3151; c) Q. Han, S. H. Bae, P. Sun, Y. T. Hsieh, Y. M. Yang, Y. S. Rim, H. Zhao, Q. Chen, W. Shi, G. Li, *Adv. Mater.* **2016**, *28*, 2253; d) J. Kim, J. S. Yun, X. Wen, A. M. Soufiani, C.-F. J. Lau, B. Wilkinson, J. Seidel, M. A. Green, S. Huang, A. W.-Y. Ho-Baillie, *J. Phys. Chem. C* **2016**, *120*, 11262; e) T. M. Koh, K. Fu, Y. Fang, S. Chen, T. Sum, N. Mathews, S. G. Mhaisalkar, P. P. Boix, T. Baikie, *J. Phys. Chem. C* **2014**, *118*, 16458; f) J. W. Lee, D. J. Seol, A. N. Cho, N. G. Park, *Adv. Mater.* **2014**, *26*, 4991; g) Z. Yang, C.-C. Chueh, P.-W. Liang, M. Crump, F. Lin, Z. Zhu, A. K.-Y. Jen, *Nano Energy* **2016**, *22*, 328.

[2] a) D. P. McMeekin, G. Sadoughi, W. Rehman, G. E. Eperon, M. Saliba, M. T. Hörantner, A. Haghighirad, N. Sakai, L. Korte, B. Rech, *Science* **2016**, *351*, 151; b) N. J. Jeon, J. H. Noh, W. S. Yang, Y. C. Kim, S. Ryu, J. Seo, S. I. Seok, *Nature* **2015**, *517*, 476.

[3] F. Wang, H. Yu, H. Xu, N. Zhao, *Adv. Funct. Mater.* **2015**, *25*, 1120.

[4] C. C. Stoumpos, C. D. Malliakas, M. G. Kanatzidis, *Inorg. Chem.* **2013**, *52*, 9019.

[5] X. Li, D. Q. Bi, C. Y. Yi, J. D. Decoppet, J. S. Luo, S. M. Zakeeruddin, A. Hagfeldt, M. Gratzel, *Science* **2016**, *353*, 58.

[6] a) M. A. Green, K. Emery, Y. Hishikawa, W. Warta, E. D. Dunlop, *Prog. Photovolt. Res. Appl.* **2016**, 24; b) H. Zhang, R. Hong, *Ceram. Int.* **2016**, *42*, 14543.

[7] M. Long, T. Zhang, Y. Chai, C. Ng, T. C. W. Mak, J. Xu, K. Yan, *Nat. Commun.* **2016**, *7*, 13503.

[8] K. Yan, M. Long, T. Zhang, Z. Wei, H. Chen, S. Yang, J. Xu, *J. Am. Chem. Soc.* **2015**, *137*, 4460.

[9] F. Hao, C. C. Stoumpos, Z. Liu, R. P. Chang, M. G. Kanatzidis, *J. Am. Chem. Soc.* **2014**, *136*, 16411.

[10] H. Yu, F. Wang, F. Xie, W. Li, J. Chen, N. Zhao, *Adv. Funct. Mater.* **2014**, *24*, 7102.

[11] W. Nie, H. Tsai, R. Asadpour, J.-C. Blancon, A. J. Neukirch, G. Gupta, J. J. Crochet, M. Chhowalla, S. Tretiak, M. A. Alam, *Science* **2015**, *347*, 522.

[12] a) R. Sheng, A. Ho-Baillie, S. Huang, S. Chen, X. Wen, X. Hao, M. A. Green, *Phys. Chem. C* **2015**, *119*, 3545; b) S. Colella,

E. Mosconi, P. Fedeli, A. Listorti, F. Gazza, F. Orlandi, P. Ferro, T. Besagni, A. Rizzo, G. Calestani, *Chem. Mater.* **2013**, *25*, 4613.
[13] S. Lv, S. Pang, Y. Zhou, N. P. Padture, H. Hu, L. Wang, X. Zhou, H. Zhu, L. Zhang, C. Huang, *Phys. Chem. Chem. Phys.* **2014**, *16*, 19206.
[14] S. D. Stranks, G. E. Eperon, G. Grancini, C. Menelaou, M. J. Alcocer, T. Leijtens, L. M. Herz, A. Petrozza, H. J. Snaith, *Science* **2013**, *342*, 341.
[15] a) J. Pan, C. Mu, Q. Li, W. Li, D. Ma, D. Xu, *Adv. Mater.* **2016**, *28*, 8309; b) J. H. Kim, S. T. Williams, N. Cho, C. C. Chueh, A. K. Y. Jen, *Adv. Energy Mater.* **2015**, *5*, 1401229; c) J. A. Aguiar, S. Wozny, T. G. Holesinger, T. Aoki, M. K. Patel, M. Yang, J. J. Berry, M. Al-Jassim, W. Zhou, K. Zhu, *Energy Environ. Sci.* **2016**, *9*, 2372.
[16] R. J. Sutton, G. E. Eperon, L. Miranda, E. S. Parrott, B. A. Kamino, J. B. Patel, M. T. Hörantner, M. B. Johnston, A. A. Haghighirad, D. T. Moore, *Adv. Energy Mater.* **2016**, *6*, 1502458.